CONF-961202--65

Presented at Fall Meeting of the Materials Research Society,
Boston, Massachusetts, December 2–6, 1996; to be published in
Atomic Resolution Microscopy of Surfaces and Interfaces,
ed. by D. J. Smith and R. Hamers, Materials Research Society,
Pittsburgh, PA, 1997

DETERMINATION OF ATOMIC STRUCTURE AT SURFACES AND INTERFACES BY HIGH-RESOLUTION STEM

S. J. Pennycook, P. D. Nellist,* M. F. Chisholm, N. D. Browning,**
D. J. Wallis,† and E. C. Dickey‡

Solid State Division, Oak Ridge National Laboratory
Oak Ridge, Tennessee 37831-6030

*Cavendish Laboratory, Madingley Road, Cambridge CB3 0HE, United Kingdom

**Dept. Physics (M/C 273), University of Illinois at Chicago
Chicago, Illinois 60607

†Defence Research Agency, Malvern, United Kingdom

‡Dept. of Materials Science and Engineering, Northwestern University
Evanston, IL 60208

SOLID STATE DIVISION
OAK RIDGE NATIONAL LABORATORY
Managed by
LOCKHEED MARTIN ENERGY RESEARCH CORP
under
Contract No. DE-AC05-96OR22464
with the
U.S. DEPARTMENT OF ENERGY
Oak Ridge, Tennessee

January 1997

DETERMINATION OF ATOMIC STRUCTURE AT SURFACES AND INTERFACES BY HIGH-RESOLUTION STEM

S. J. PENNYCOOK, P. D. NELLIST*, M. F. CHISHOLM, N. D. BROWNING**, D. J. WALLIS*** AND E. C. DICKEY****
Solid State Division, Oak Ridge National Laboratory, Oak Ridge, Tennessee 37831-6030
*now at Cavendish Laboratory Madingley Road, Cambridge CB3OHE, UK
**Department of Physics, University of Illinois at Chicago, Chicago, IL 60607-7059
***now at Defence Research Agency, Malvern, UK
****Dept. of Materials Science & Engineering, Northwestern University, Evanston, IL 60208

INTRODUCTION:

It is just over one hundred years since Lord Rayleigh first showed the differences between coherent and incoherent imaging in the light microscope, pointing out the advantages of the latter for resolution and image interpretation. The annular detector in the high-resolution STEM provides the same advantages for electrons, allowing incoherent imaging at atomic resolution, with image contrast strongly dependent on atomic number (Z). Since incoherent imaging has no phase problem, these Z-contrast images may be directly inverted to give the (projected) atomic positions. A maximum entropy method avoids false detail associated with direct deconvolution, and gives atomic coordinates to an accuracy of ± 0.1 Å. Electron energy loss spectroscopy can provide valuable complementary information on light element bonding and the presence of impurities in specific atomic planes selected from the image. Together, these techniques have revealed some surprisingly complex interfacial structures. For surface studies, the 1.3 Å probe of the VG Microscopes HB603U STEM provides sufficient penetration and contrast to image single Pt and Rh atoms on γ-alumina supports. Such images reveal preferred atomic configurations, and allow possible surface adsorption sites to be deduced.

INCOHERENT IMAGING WITH ELECTRONS

Lord Rayleigh was the first to show clearly the difference between imaging with coherent illumination, when fixed definite phase relationships exist between the illumination at various points on the object, and incoherent imaging, in which there are no fixed phase relationships in the illumination [1]. In this latter case the image can only depend on the intensity of illumination at each point in the object, just as if the object were self-luminous. His famous diagram, reproduced in Fig. 1, shows the amplitude in the image plane resulting from transfer through the objective lens for two point objects, illuminated coherently and incoherently. The two points are spaced such that the peak of the Airy disc from one falls at the first zero in the Airy disc of the other. If the two points are illuminated in phase, then they are unresolved, but become resolved for incoherent illumination. The third case, for illumination that is 180° out of phase on the two objects, always resolves the objects, but this obviously cannot be accomplished in practice for a range of object spacings.

Lord Rayleigh also appreciated the role of the condenser lens: "It seems fair to conclude that the function of the condenser in microscopic practice is to cause the object to behave, at any rate in some degree, as if it were self-luminous, and thus to obviate the sharply-marked interference bands which arise when permanent and definite phase relationships are permitted to exist between the radiations which issue from various points of the object". By illuminating over a large angular range the degree of phase correlation between different points on the object can be reduced to a minimum. In light optical imaging, if the objective lens aperture is made as large as possible for the best resolution, then the condenser lens aperture cannot be made larger still. Thus, at the limit of resolution, some phase correlations must exist, and we would expect to see some quantitative departures from incoherent imaging theory.

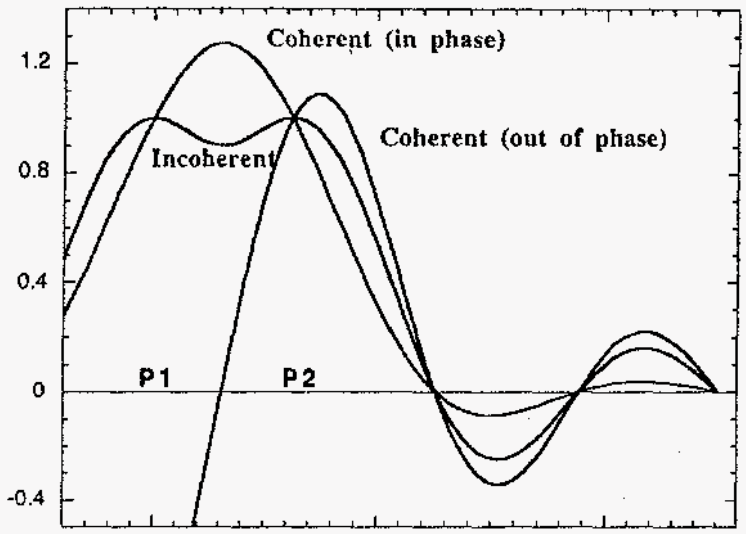

Fig. 1. Image amplitude for two point objects P1 and P2 illuminated coherently (in phase and 180° out of phase) and with incoherent illumination, after Lord Rayleigh [1].

In the STEM, the optical equivalent of the condenser lens is, by reciprocity, a large axial detector. However, since electrons are not absorbed by the specimen, only scattered, the contrast in such a detector would be quite weak, and it is advantageous to use an annular detector. With a large outer radius, such a detector will give a complementary image by Babinet's principle, and it can therefore be considered as optically equivalent to the condenser lens of the light microscope. An important advantage however is that the detector is just a detector, not a lens, and so the inner radius can be made as large as desired to achieve the ideal of a self-luminous specimen as closely as necessary. In practice, calculations have shown that when imaging a spacing d, an inner detector angle of $1.22\lambda/d$ will result in image intensities within 5% of those calculated by incoherent imaging theory. [2]

It is also clear that if the Rayleigh detector is destroying phase correlations effectively, by detecting the total intensity from the large number of overlapping discs falling on it, then it will also be insensitive to multiple scattering between the discs. Transferring intensity from one part of the diffraction pattern to another will not affect the integrated signal provided there is no net scattering on or off the detector. This is precisely how dynamical diffraction manifests itself, and is the reason that incoherent imaging theory works even in crystals of significant thickness. The first detailed calculation of dynamical effects showed how it was only the s-type Bloch states that were excited in phase at all angles within the incident STEM probe, other states that may be strongly excited on axis, being greatly reduced in effectiveness once the angular integration over the probe was performed. This provided an explanation for the lack of significant thickness fringes and other dynamical effects, and led to an expression for the thickness dependence of the dynamical object function [3-5]. However, incoherent imaging was assumed, in that the image intensity was taken to be proportional to the electron intensity at the atomic sites. Detailed calculations by other authors have confirmed this assumption is valid at high detector angles [6]. More recently, a reciprocal space formulation has been developed which removes this assumption, and shows clearly how even in the presence of dynamical diffraction, integrating the overlapping diffraction discs on the detector leads to incoherent imaging. This formulation shows explicitly the degree of coherence between different Bloch states, and how this changes with thickness and detector inner cutoff. [7]

PROBE AND OBJECT RECONSTRUCTION

Figure 2 shows a Z-contrast image of NiO along the [112] zone axis taken with the VG Microscopes HB603U showing that the 1.47Å {220} spacing is clearly resolved [8]. The Fourier transform of the image intensity shows in addition a weak spot corresponding to the {311} spacing at 1.26Å. Thus we are transferring information at the expected Scherzer resolution limit of 0.43 $C_s^{1/4}$ $\lambda^{3/4}$ [9], which is in fact 1.26Å, for 300 kV and 1 mm spherical aberration coefficient. This demonstrates the resolution improvement expected for a Rayleigh detector, as the objective aperture did not contain either the 1.47Å or 1.26Å spacings.

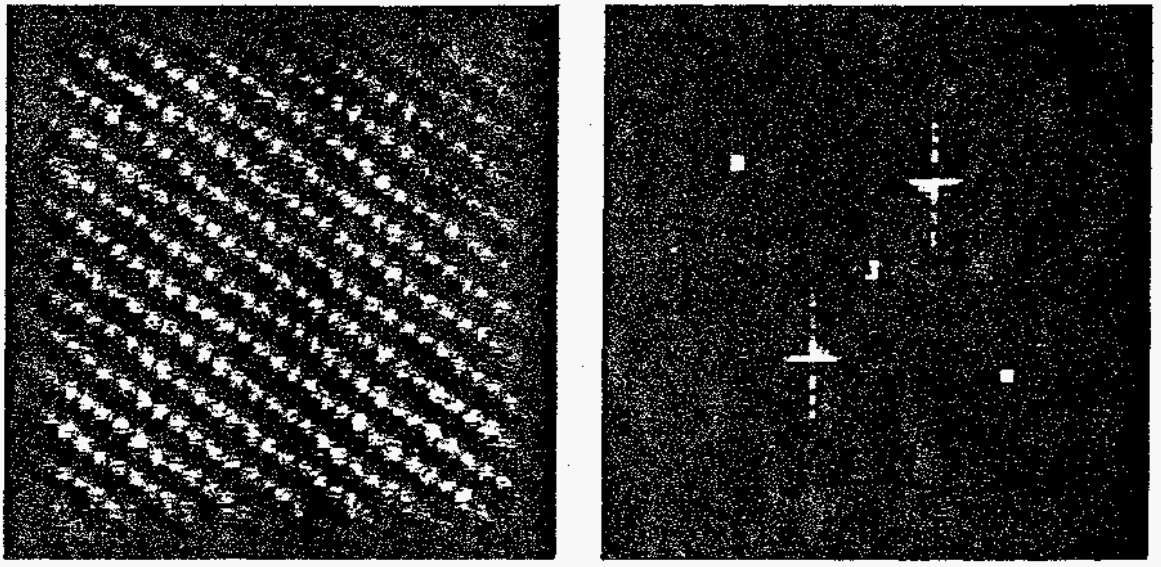

Fig. 2. Image of NiO in the [112] projection with Fourier transform showing transfer down to 1.26 Å.

The resolution cutoff for incoherent imaging is double that of coherent imaging for a given objective aperture size, as can be seen from Fig. 3. For coherent phase contrast imaging, a small axial bright field detector is used, equivalent by reciprocity to a small condenser aperture in the light microscope and conventional TEM. Fringes result only if the corresponding diffracted beams are present in the objective aperture, i.e. the resolution limit is the objective aperture radius. With the annular detector, disc overlaps are present on the detector provided the diffraction discs are spaced less than the *diameter* of the objective aperture, resulting in double the resolution.

The intensities in the Fourier transform of Fig 2 can be compared to those expected for perfect incoherent imaging to obtain the microscope transfer function, as shown in Fig. 4 [10]. It is interesting to note that the transfer selected by the user as the best focus condition is in fact very similar to the optimum transfer function. Presumably the eye is used to smaller spacings having less contrast than larger spacings from everyday experience, and tunes the microscope focus appropriately. Figure 5 shows the reconstructed probe intensity profile (the transform of the measured transfer function) which is only slightly broader than the theoretical probe profile. To reconstruct the object from the image it is best to use a maximum entropy technique. The constraint of maximum entropy, roughly equivalent to a criterion of minimum object detail consistent with the image, is effective in removing from the image any false detail resulting from the probe tails. These tails are clearly seen in the theoretical and reconstructed probes in Fig. 5, and a good example of false detail is seen in the image of GaAs shown in Fig. 6a. A small secondary maximum is visible between the dumbbells because when the probe is at this position the probe tail peaks on the six surrounding columns. The object retrieved by the maximum entropy method, Fig. 6b, removes this feature because the correct object has a lower entropy

than one containing additional columns. A conventional deconvolution does not have this property since it only enhances image detail up to the resolution limit, followed by a sharp truncation of transfer in Fourier spacing, which results in enhanced false detail [9]. The reconstruction corrects the dumbbell spacing, which is somewhat elongated in the raw image as a result of the limited high spatial frequency transfer. Column positions are retrieved to within ± 0.1 Å of their true positions, a limit set by the noise statistics.

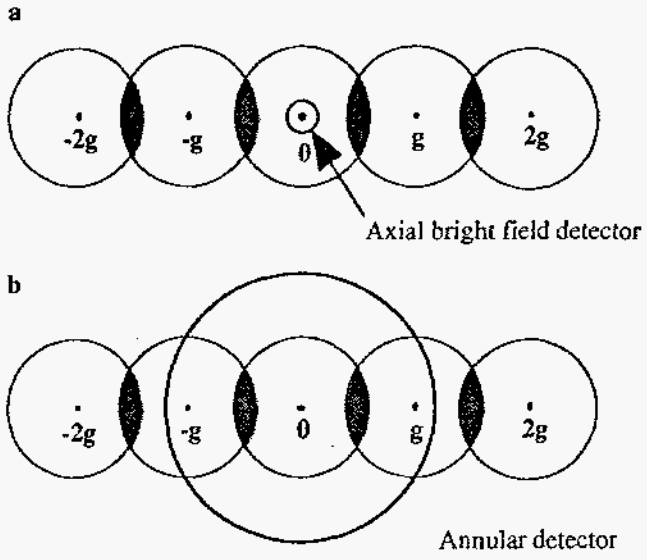

Fig. 3. Regions of overlapping convergent beam discs for a diffraction vector greater than the objective aperture radius. (a) An axial bright field detector shows no contrast, while in (b), regions of overlapping discs fall on the annular detector .

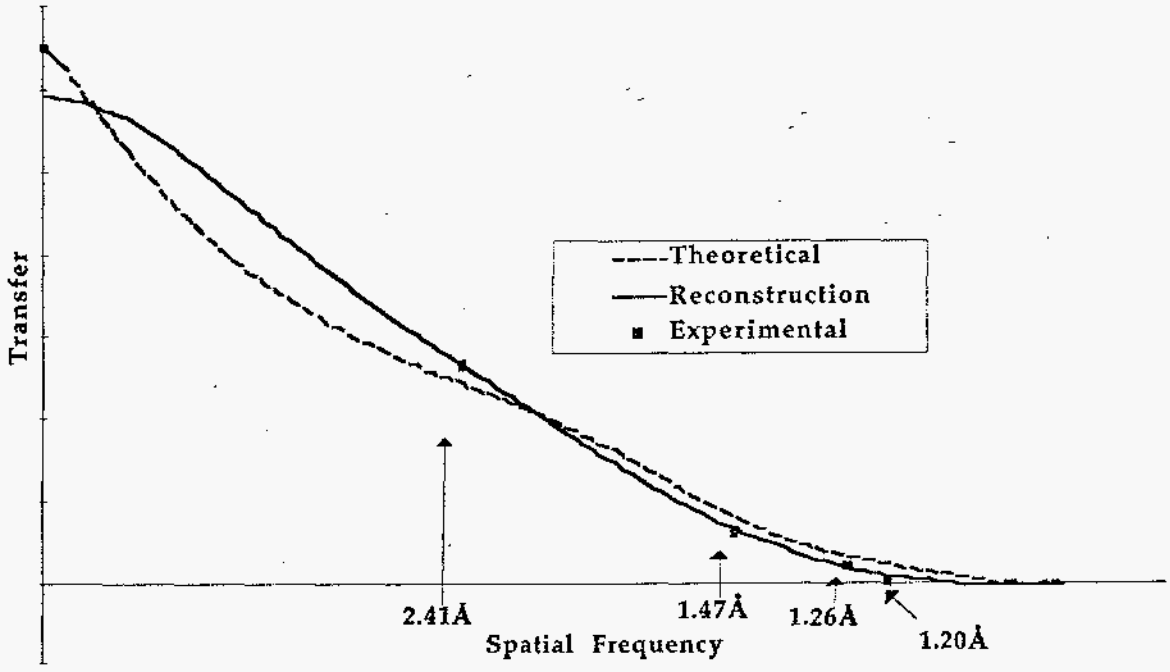

Fig. 4. Reconstructed microscope transfer function obtained from NiO [112], compared to theoretical optimum (dashed).

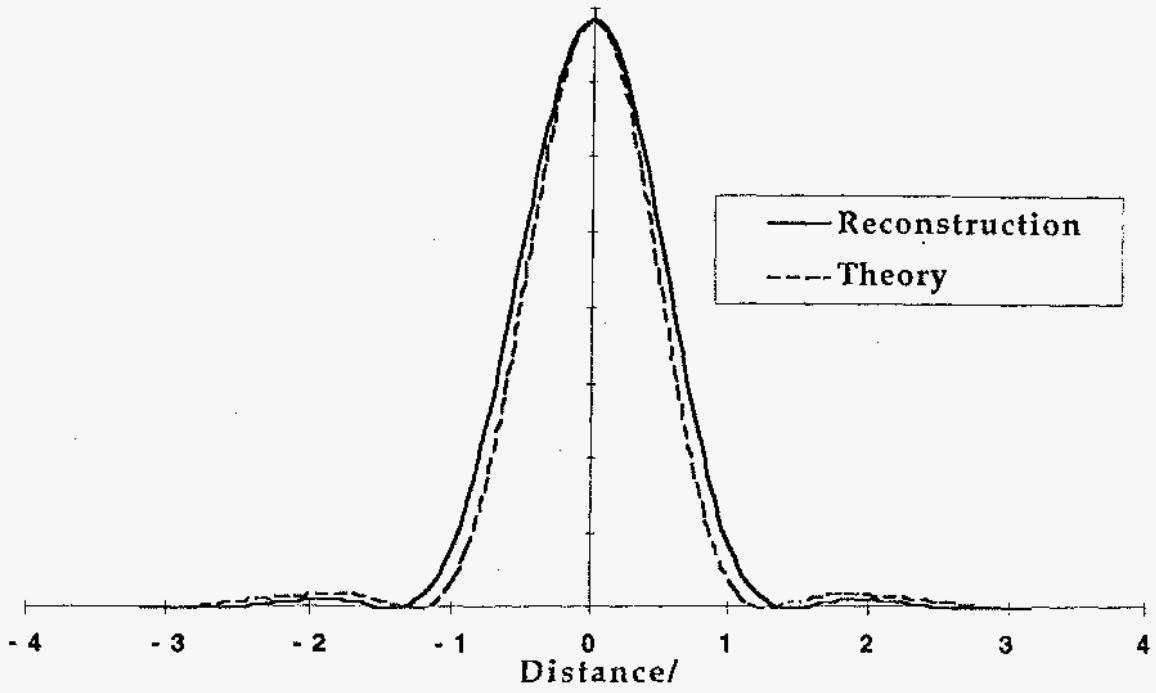

Fig. 5. Reconstructed microscope probe intensity profile obtained from NiO [112], compared to theoretical optimum (dashed).

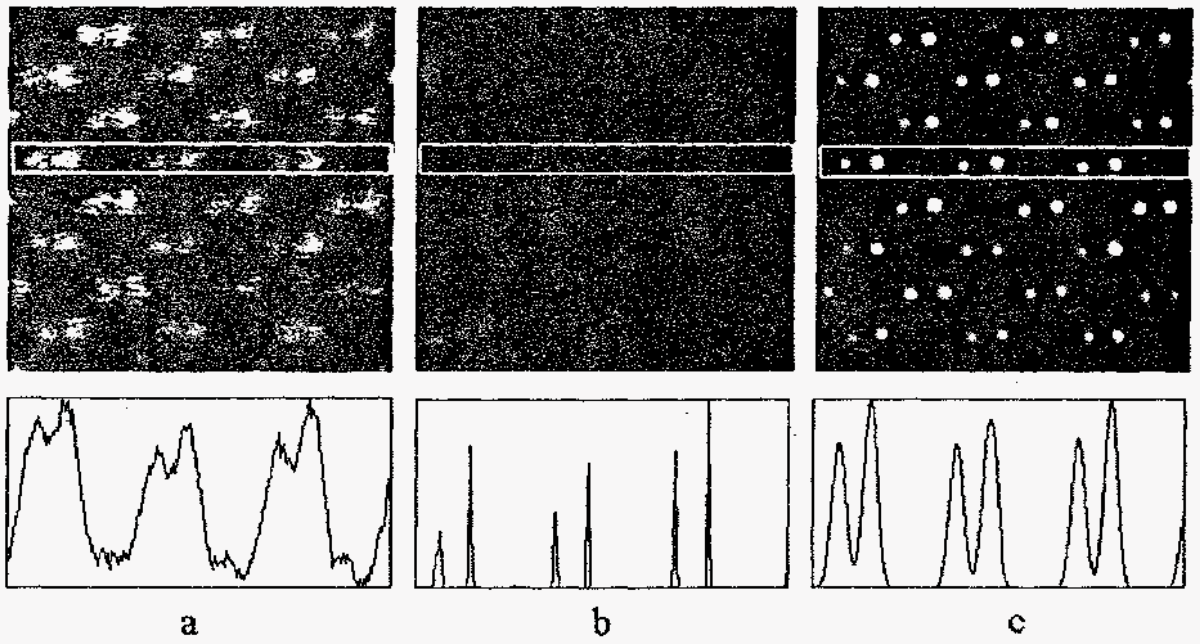

Fig. 6. Image of GaAs [110] showing, (a) raw image, with As columns showing the expected ~10% higher scattering power, (b) maximum entropy reconstruction of the object, (c) a reconstructed image. Line traces below show the vertically averaged intensity within the rectangles outlined.

APPLICATION TO INTERFACES

The ability to invert the image directly to the most likely object, coupled with the sensitivity to sublattice polarity apparent from Fig. 6, is of great value in studying semiconductor interfaces. For example, it has proved possible to image the core structures of dislocations at a CdTe/GaAs interface [11], and to locate the cores with respect to the interface plane. 60° dislocations were shown to be of glide type, while perfect edge (Lomer) dislocations were found to have either the Hornstra structure showing as five- and seven- fold rings in projection, or a new structure comprising a four-fold core surrounded by distorted six-fold rings.

A particularly complex and unexpected interfacial structure has recently been found at CdTe/Si interfaces grown by a particular molecular beam epitaxy growth procedure [12]. From Fig. 7, it is immediately clear that the CdTe film is terminated by Te. In addition, for several monolayers into the Si substrate, occasional columns show brighter than the surrounding Si, although remaining in the correct position. Suggestive of interdiffusion from the film, this is not the case, as was determined by EELS performed plane by plane across the interface using a VG Microscopes HB501UX. The Cd M_{45} edge decreased to zero by the second Si plane, whereas the Te M_{45} edge continued to be detected to a depth of 4 or 5 {200} layers. The presence of Te was presumably caused by flooding the Si wafer with Te after cleaning, while still at high temperature. The temperature was then reduced significantly for growth, explaining the lack of Cd diffusion. Thus we can identify each bright spot in the image with a few (or possibly single) atoms of Te located substitutionally in that particular Si column. Careful observation of the relative positions of the Te and Si columns across the interface shows no sign whatsoever of localized interface dislocations, leading to the surprising conclusion that the interface is incommensurate. This conclusion is backed up by a maximum entropy measurement of the separation of these two planes; at 3.2 Å, the spacing is too high for strong covalent bonds to form, consistent with the incommensurate interface deduced from the image.

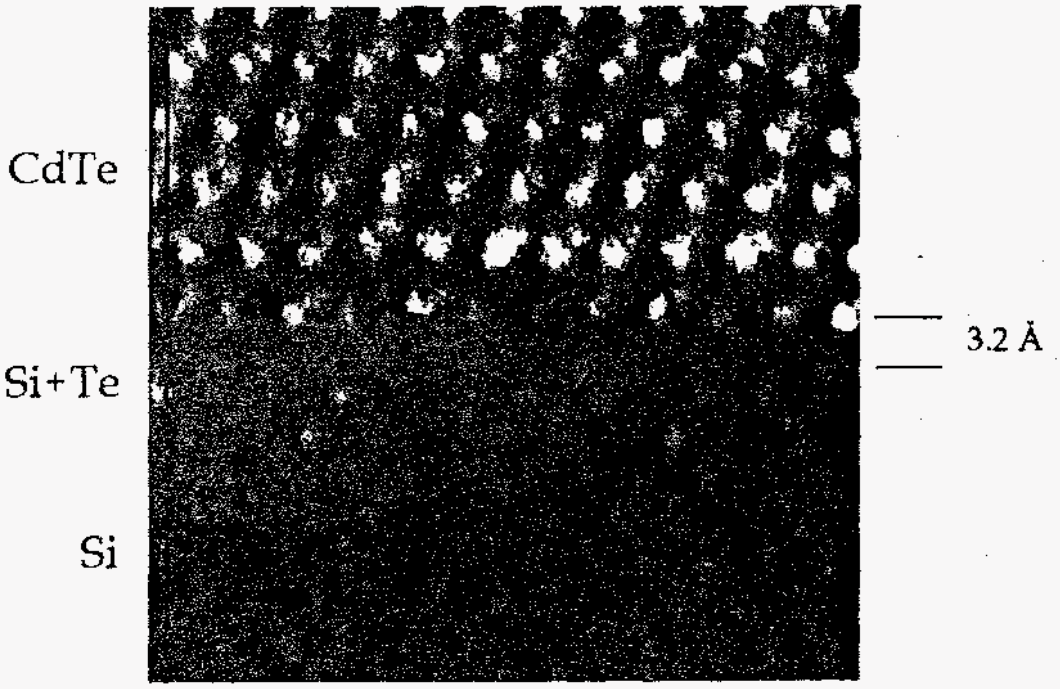

Figure 7. Z-Contrast image of a CdTe(111)/Si(100) interface showing its incommensurate nature.

APPLICATION TO SURFACES

Evidence of the visibility of small numbers of heavy impurity atoms in Si columns is seen in Fig. 7. Individual atoms are expected to be visible when their atomic number is high enough to give a sufficient increase in scattering to be detectable over the signal from the matrix. In catalysis, it is often the case that heavy elements are distributed on light supports such as γ-alumina. With 100 kV instruments, single atoms did not give sufficient signal to be seen above the background of the support, but with a 300 kV STEM this now becomes possible. Figure 8 shows Pt atoms and small clusters supported on γ-alumina [13]. Not visible in conventional bright field images, the larger bright patches correspond to small three-dimensional clusters that are not resolved, while the smallest bright spots correspond to individual Pt atoms. From fringes seen in the bright field image, obtained simultaneously, it was possible to determine the orientation of the support, and so to determine the surface on which the Pt was sitting. A particularly common configuration was that of a trimer, shown circled, in which the spacings and angles were significantly altered from a close packed equilateral triangle. This is indicative of strong interaction with the support, and allows the likely atomic sites to be determined as shown in Fig. 8b. Note that such a trimer cannot straddle a surface step or one of the three atoms would be too far away from the others to be bonded, and therefore we would not expect to see a predominance of trimer configurations in the images. This means that we are imaging the initial stages of the nucleation of the Pt clusters. Subsequently, the clusters grow three-dimensionally, and we can only image larger clusters that are well-oriented with the electron beam.

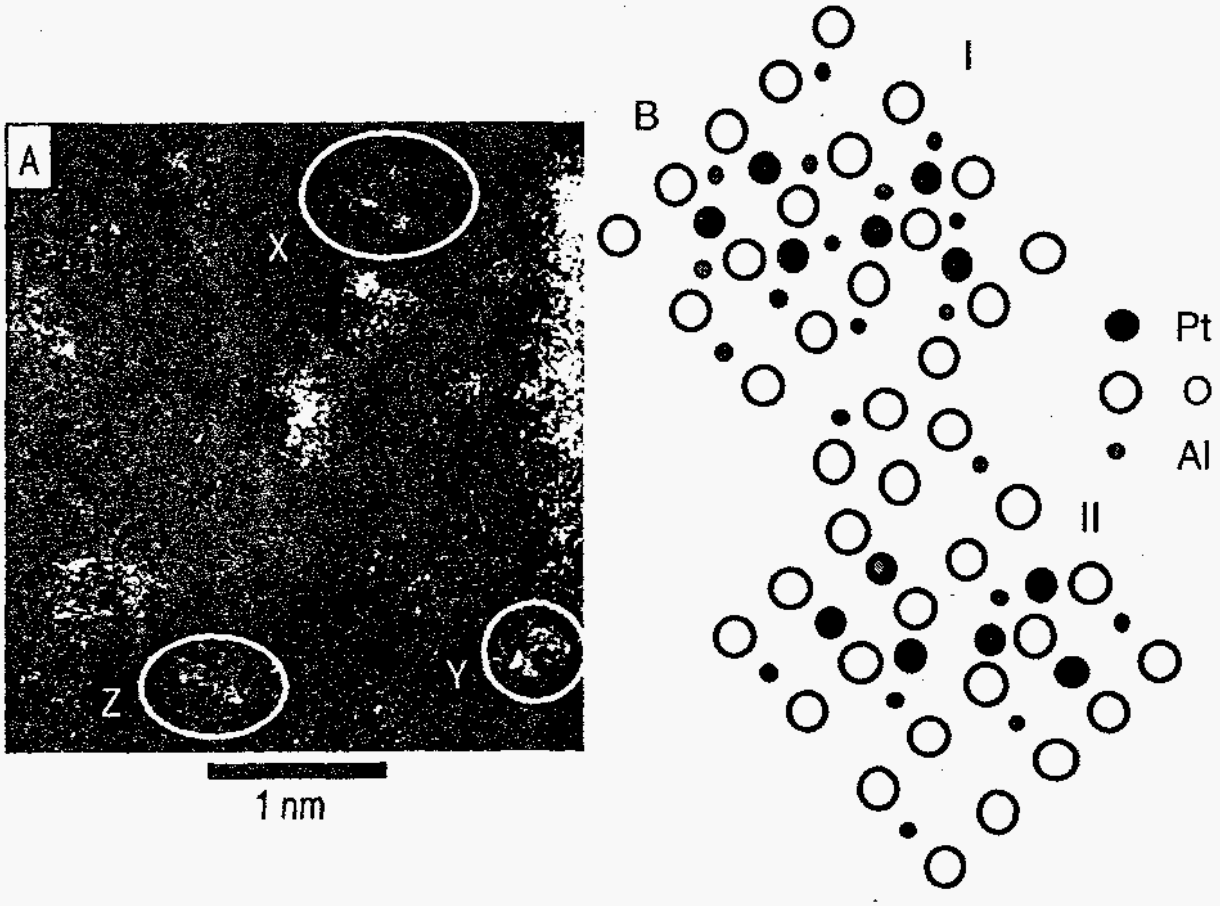

Fig. 8. (A) Z-contrast image of Pt atoms on γ-alumina after bandpass filtering to remove thickness variations and noise. Trimer X has a configuration that is constrained to match the two possible {110} surfaces of the support (B). Dimers Y and Z each match one side of trimer X.

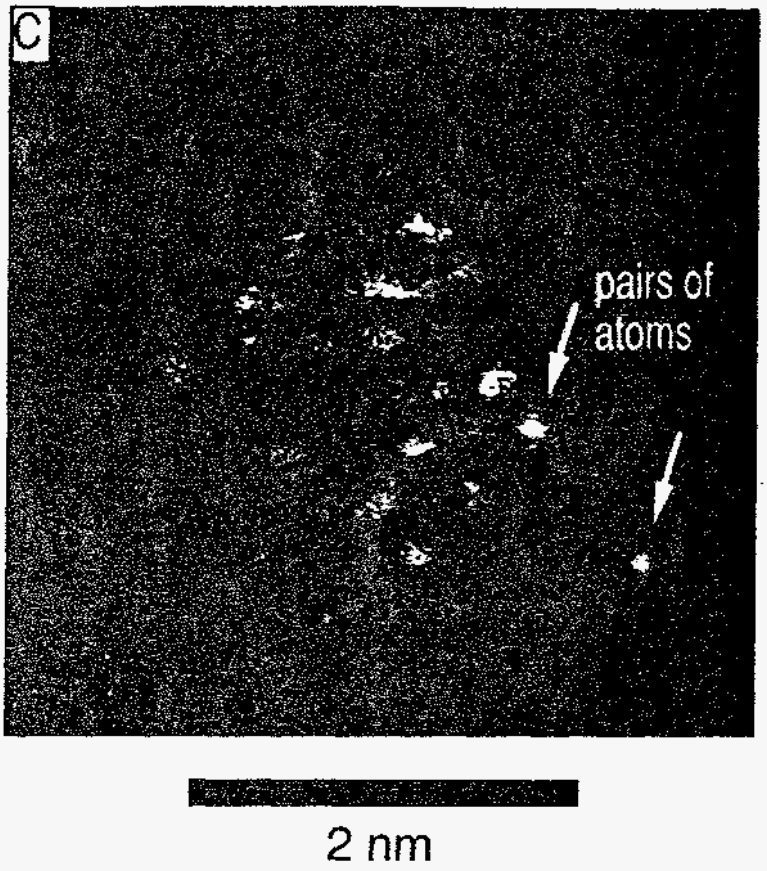

Fig. 9. (a) Z-contrast image showing a raft of Rh atoms on γ-alumina. Arrows point to spots whose intensity corresponds to two Rh atoms in projection.

The behavior of Rh supported on γ-alumina is surprisingly different. In Fig. 9 we see a small patch of Rh atoms revealed in the Z-contrast image. Most of the bright features are single atoms, but some are distinctly more bright, and correspond to two atoms aligned approximately with the beam direction. One of these pairs is quite separate from the remainder of the raft, which suggests that the Rh is extending downwards into the support rather than outwards into three-dimensional clusters. The striking difference from Pt is clear: Rh has a strong tendency to form extended rafts and to dissolve into the substrate. Such differences must be caused by the different activation energies of surface and bulk diffusion, and must at least partly be responsible for the different catalytic and aging behavior of the two species.

FUTURE DIRECTIONS

Instrumentally, the addition of an EELS capability to a high voltage STEM would result in a most powerful combination, allowing the improved resolution and much greater penetrating power to be exploited for spectroscopy as well as imaging. The sensitivity of EELS measurements to details of the interfacial structure would be enhanced, and we can expect to see increasing use of EELS fine structure simulations as an aid in refining interface structure and impurity site location. There would also seem to be significant advantage in increasing the accelerating voltage somewhat further. At 400 kV, with a good objective lens, it should be possible to achieve Scherzer resolution limits of below 1 Å, giving significant gains in image contrast, particularly for light atoms.

The ability of the STEM to image surface atomic sites on insulating supports provides another powerful capability, with potential applications to catalysis. The addition of a reaction

chamber and a hot stage to a high voltage STEM should elucidate many details of the metal/support interactions that are central to catalytic activity but currently hidden from study.

These STEM techniques also have a powerful synergy with theoretical studies. Our ability to determine many details of interfacial and surface structure directly from experiment allows *ab initio* total energy calculations to be used to great efficiency [14]. No longer is it necessary to perform painstaking and time-consuming searches of all possible structures. It is just becoming possible for first principles theory to handle the large numbers of atoms needed to model real systems, just as we are able to study local systems in unprecedented detail. Such a combined experimental and theoretical effort is necessary to understand the structure/property relations at interfaces, relations that are at the heart of the electrical, optical and mechanical properties of many advanced materials.

ACKNOWLEDGMENTS

The authors are grateful to A. G. Norman, V. P. Dravid, D. R. Liu, and E. Lowenthal for provision of samples, and to J. T. Luck for technical assistance. This research was sponsored by the Division of Materials Sciences, U.S. Department of Energy, under contract DE-AC05-96OR22464 with Lockheed Martin Energy Research Corporation, and in part by ORNL's Laboratory Directed Research and Development Fund and appointments to ORNL Postdoctoral Research Program administered by the Oak Ridge Institute for Science and Education.

REFERENCES

1. Lord Rayleigh, Phil. Mag. (5) **42** 167 (1896).
2. D. E. Jesson and S. J. Pennycook, Proc. R. Soc. Lond. **A441** 261 (1993).
3. S. J. Pennycook and D. E. Jesson, Phys. Rev. Lett. **64** (1990) 938.
4. S. J. Pennycook and D. E. Jesson, Ultramicroscopy **37** 14 (1991).
5. S. J. Pennycook and D. E. Jesson, Acta Metall. Mater. **40** Suppl. S149 (1992).
6. R. F. Loane, P. Xu and J. Silcox, Ultramicroscopy **40** (1992) 121
7. P. D. Nellist and S. J. Pennycook, Phys. Rev. Lett., submitted.
8. E. C. Dickey et. al., Acta Metall. Mater, in press, (1997).
9. O. Scherzer, J. Appl. Phys. **20** 20 (1949).
10. P. D. Nellist and S. J. Pennycook, Scanning Microscopy Supplement II, in press (1997).
11. A. J. McGibbon , S. J. Pennycook and J. E. Angelo, Science **269**, 519 (1995).
12. Y.P. Chen, J.P. Faurie, S. Sivananthan, G.C. Hua and N. Otsuka, J. of Electronic Materials **24** 475 (1995).
13. P. D. Nellist and S. J. Pennycook, Science **274** 413 (1997).
14. M. F. Chisholm, A. Maiti, S. J. Pennycook and S. T. Pantelides, Science, submitted.